Available online at www.sciencedirect.com
ScienceDirect
Trans. Nonferrous Met. Soc. China 34(2024) 1922−1935
Transactions of Nonferrous Metals Society of China
www.tnmsc.cn

Effect of Ag content on microstructure and mechanical properties of Sn−*x*Ag−0.5Cu solder joints under rapid thermal shock

Chen PENG[1], Shan-lin WANG[1], Ming WU[1,2], Li-meng YIN[3],
Yu-hua CHEN[1], Ke-jiang YE[1], Wei-zheng CHEN[1], Ti-ming ZHANG[1], Ji-lin XIE[1]

1. Jiangxi Key Laboratory of Forming and Joining Technology for Aerospace Components, Nanchang Hangkong University, Nanchang 330063, China;
2. Jiangxi Intelligent Industry Technology Innovation Research Institute, Nanchang 330200, China;
3. School of Metallurgy and Materials Engineering, Chongqing University of Science and Technology, Chongqing 401331, China

Received 6 December 2022; accepted 15 May 2023

Abstract: The effects of Ag content on the microstructure and shear strength of Sn−*x*Ag−0.5Cu solder joints under rapid thermal shock were investigated using high-frequency induction heating equipment. The results show that the increased Ag content can make the surface of the solder joint denser and smoother and reduce the generation of long strips of Cu_6Sn_5 intermetallic compound (IMC) inside the solder joint, thus enhancing the oxidation resistance of the solder joint. Ag accelerates the growth rate of the IMC layer at the solder joint interface, the growth rate of the Cu_6Sn_5 layer is determined by both bulk diffusion and grain boundary diffusion, and the growth rate of the Cu_3Sn layer is determined by both bulk diffusion and interfacial reaction. In the rapid thermal shock environment, the fracture mode of the solder joint converts from ductile fracture to brittle fracture. At the same time, the high Ag content shortens the fracture mode transition time of the solder joint and reduces the thermal fatigue resistance of the solder joint.

Key words: Ag content; rapid thermal shock; Sn−Ag−Cu; solder joints; growth kinetics; fracture mode

1 Introduction

The application of traditional Pb−Sn solder is hindered by its polluting Pb content [1], and Sn−Ag−Cu (SAC) lead-free solder is widely used in the electronics industry as an alternative to Pb−Sn solder [2−5]. Compared to traditional Pb−Sn solder, Sn−Ag−Cu (SAC) lead-free solder is expensive, which prevents the broader use of high Ag content SAC lead-free solder. However, if the Ag content of the solder is reduced to save solder cost, a series of problems will occur, for example, the increased melting temperature of the solder, decreased spreading rate [6], deteriorated wetting performance [7], electromigration resistance [8], and strength [9], among others. Therefore, there is a need to study the differences in the microstructure and mechanical properties of Sn−Ag−Cu alloys with different Ag contents to reduce the Ag content and achieve cost reduction while ensuring the reliability of solder joints.

SYED et al [10] found that the reliability of SAC solder joints in temperature cycling tests increased with increasing Ag content. When the Ag content was 3.0−3.2 wt.%, the solder joints showed good temperature cycling reliability, and the service strength, tensile strength, and shear

Corresponding author: Shan-lin WANG, Tel: +86-13755603426, E-mail: slwang70518@nchu.edu.cn;
Yu-hua CHEN, Tel: +86-13330067995, E-mail: ch.yu.hu@163.com
DOI: 10.1016/S1003-6326(24)66516-7
1003-6326/© 2024 The Nonferrous Metals Society of China. Published by Elsevier Ltd & Science Press
This is an open access article under the CC BY-NC-ND license (http://creativecommons.org/licenses/by-nc-nd/4.0/)

strength all showed maximum values. When the Ag content exceeded 3.2 wt.%, the mechanical properties of the solder joint no longer changed significantly. CHE et al [11] performed tensile tests on Sn−*x*Ag−0.5Cu (*x*=1, 2, and 3, wt.%) solders and found that higher Ag contents corresponded to higher solder strength and lower solder ductility. Therefore, high Ag-content SAC solder joints had poor drop resistance.

The modern microelectronics industry is moving toward high performance, high power, and integration. The size of microsolder joints in components will be less than 20 μm, leading to a significant increase in the heat flow density of electronic packages [12]. Due to different thermal expansion coefficients of the components in the packaged devices and the effect of stress, thermal fatigue damage occurs in the solder joints [13], especially in insulated gate bipolar transistor (IGBT)-type high-power devices [14]. The environment in which components are used has become severer, and people are therefore demanding higher thermal reliability of solder joints in components [15]. Conventional temperature cycling tests have a low number of cycles and a low-temperature change rate, mainly with thermal cycling rates less than 20 °C/min and thermal shock rates no less than 30 °C/min [16]. Compared to thermal cycling, thermal shock reflects the changes in solder joints under high-power, and high-performance operating conditions.

Electromagnetic induction heating (EMIH) is a noncontact heating method that relies on the principle of electromagnetic induction to heat metals directly through the eddy current effect. ZHANG et al [17] studied the changes in SAC305 solder joints during thermal shock by electromagnetic induction heating and found that fatigue cracks appeared first at the boundaries of the joints in this environment, which became webbed and spread throughout the joints after 72 h of thermal shock. However, under the conventional thermal shock and thermal cycling tests, SAC solder joints showed only minor cracks at the solder−substrate connection [18]. TIAN et al [19] compared the effects of conventional and electromagnetic induction thermal shocks on solder joints and found that the latter caused large and deep cracks. This is because the rapid thermal shock generated by induction heating brings about faster temperature changes in the solder joint, resulting in increased thermal stress and contributing to the development of cracks.

The above study shows that the rapid thermal shock generated by induction heating significantly affects the microstructure, morphology, and properties of Ag-containing materials. In contrast, more research must be conducted on materials with different Ag contents under rapid thermal shock conditions generated by induction heating. Therefore, the macroscopic morphology, microstructure, evolution of interfacial IMC, and shear strength of Sn−*x*Ag−0.5Cu solder joints with different Ag contents were investigated under the test conditions of rapid thermal shock generated by induction heating to investigate the thermal reliability of high Ag (4 wt.%) and low Ag (1 and 2 wt.%) solder joints under a rapid thermal shock environment.

2 Experimental

SAC105, SAC205, and SAC405 BGA solder balls and copper-plated printed circuit board (PCBs) were used for the experiments. In this study, the average roundness of all three solder balls used was 0.1, the average diameter was 600 μm, and the specific composition and properties are given in Table 1. The total thickness of the substrate is 600 μm, the thickness of copper is 35 μm, and the final solder resist layer made is approximately 15 μm. In the reflow soldering of solder joints using a TYR108C-type lead-free reflow machine, the temperature profile during soldering is divided into

Table 1 Chemical composition and physical properties of solder balls

Solder	Chemical composition/wt.%			Physical properties			
	Sn	Ag	Cu	Melting point/°C	Density/ ($g\cdot cm^{-3}$)	Thermal conductivity/ ($W\cdot m^{-1}\cdot K^{-1}$)	Resistivity/ ($\mu\Omega\cdot m^{-1}$)
SAC105	98.5	1.0	0.5	219	7.32	60	0.133
SAC205	97.5	2.0	0.5	218	7.34	59	0.132
SAC405	95.5	4.0	0.5	217	7.40	62	0.132

four parts: the pre-heating zone, holding zone, reflow zone, and cooling zone, where the peak temperature is 250 °C. The solder joints were held at the peak temperature for 5 s and stayed above the liquid phase line for 95 s.

In experiment with a high-frequency thermal shock rate, high-frequency induction heating equipment was selected as the heat source. High-frequency induction heating is a noncontact method based on the principle of electromagnetic induction, which directly heats the metal through the eddy current effect. SP−40AB high-frequency induction heating equipment and homemade auxiliary devices were used for the test. The solder joints and working platform were quickly cooled using flowing circulating water, as shown in Fig. 1. The test temperature profile is shown in Fig. 2, where the low temperature is 35 °C, the high temperature is 180 °C, the temperature rise time is 10 s, the temperature rise rate is 14.5 °C/s, the temperature drop time is 124 s, and the temperature drop rate is 1.17 °C/s. The low-temperature insulation is 5 s, the thermal shock cycle is 144 s, and the total cycle time is 72 h.

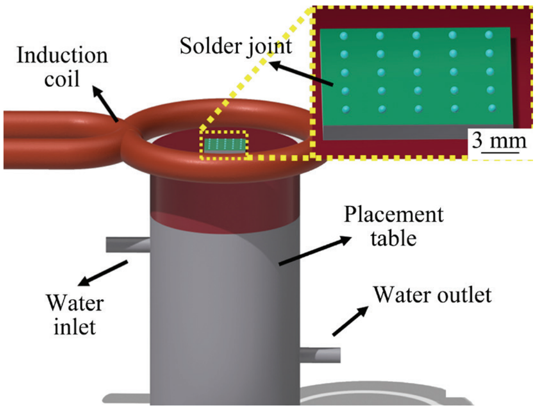

Fig. 1 Schematic diagram of thermal shock test device

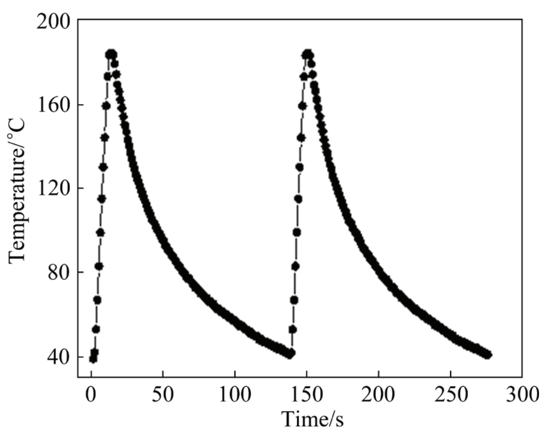

Fig. 2 Temperature profile of thermal shock experiment

Metallographic samples of Sn−*x*Ag−0.5Cu solder joints with different Ag contents were prepared after thermal shock tests to study and analyze the internal microstructure of the solder joints and the formation and evolution of the interfacial intermetallic compound (IMC) layer. Since the melting points of all three types of weld balls are below 220 °C, the samples were made using the cold mosaic method. The specimens were etched with 5% HCl + C_2H_5OH for 10−15 s, after which they were cleaned and blown dry to observe the interfacial IMC. To study the influence of IMCs inside the solder joint on the macroscopic morphology of the solder joint and the growth of IMCs at the interface during thermal shock, HCl, HF and C_2H_5OH were used to corrode the solder joint deeply, and the base of the solder joint is gradually corroded away. When the internal IMC of the solder joint and the interface IMC are exposed, the corrosion is stopped, and the joint is cleaned by ultrasonic cleaning in an alcohol solution and then blown dry.

The internal microstructure of the solder joints and the IMC interface microstructure were observed and analyzed with a field scanning electron microscope (FSEM) from Phenom, and the elemental composition of the solder joints was analyzed with an energy-dispersive spectrometer (EDS). An MFM 1200 push-pull tester was used for shear testing of solder joints with different Ag contents, where the displacement rate was 400 μm/s, and the height was 40 μm. The maximum shear forces F_i on the solder joint and the solder joint area A_i were measured, and the shear strength τ of the solder joint was calculated as follows:

$$\tau=\frac{1}{N}\sum_{i=1}^{N}\frac{F_i}{A_i} \tag{1}$$

where τ is the average shear strength of the solder joint (MPa), N is the number of solder joints, F_i is the maximum shear force of the solder joint (N), and A_i is the area of the solder joint (mm^2). The average of five solder joints was taken as the shear strength.

The fracture morphology of the solder joints after the shear test was observed to determine the fracture location of each solder joint as well as the fracture type to assess the effect of thermal shock on the fracture pattern of the solder joints with different Ag contents.

3 Results and discussion

3.1 Evolution of macroscopic shape of solder joint

The macroscopic morphology of the solder joints with different Ag contents before the rapid thermal shock is shown in Fig. 3.

As the Ag content increased, the solder joint roughness decreased, and the solder joint surface gradually tended to be smooth and tight. From Figs. 3(a−c), it can be seen that the solder joints with various Ag contents exhibited good formation. The size of the Sn particles on the solder joint surface shrank from 3−5 μm in SAC105 to 1−3 μm in SAC405 joints, and the spacing between the Sn particles also shrank, as shown in Figs. 3(d−f).

The rapid thermal shock caused oxidation of the solder joint, which changed the macroscopic morphology of the joint [20]. Under rapid thermal shock, high Ag-content solder joints had fewer holes and cracks and were less susceptible to oxidation. The macroscopic morphology of the solder joints with different Ag contents at various rapid thermal shock time is shown in Fig. 4. After 18 h, the surface of the SAC105 solder joint became rough, and many tiny holes appeared, as shown in Fig. 4(a). As the rapid thermal shock continued, the roughness of the solder joint surface increased, and the surface holes became larger, as shown in Figs. 4(b, c). Holes also appeared on the surface of the SAC205 solder joint after 18 h of rapid thermal shock, with a raised strip on the top of the solder joint, as shown in Fig. 4(d), which was confirmed by EDS inspection to be the intermetallic compound of Cu_6Sn_5. The Cu_6Sn_5 strips running through the solder joints grew, with a width of approximately 30 μm, as shown in Figs. 4(e, f). Compared to the first two types of solder joints, the morphology of the SAC405 solder joints was least affected by rapid thermal shock (Figs. 4(g−i)). The morphological changes in the SAC405 solder joints after 18 h of rapid thermal shock were slightly changed, and even after 72 h, there were no coarse holes in the SAC405 solder joints.

As the Ag content increased, the size of the Sn particles on the surface of the solder joint decreased, making the surface of the solder joint denser; therefore, the interior of the solder joint was less susceptible to oxidation by oxygen. In addition, the increased Ag content enhanced the corrosion resistance of Sn-based solders [21]. It promoted

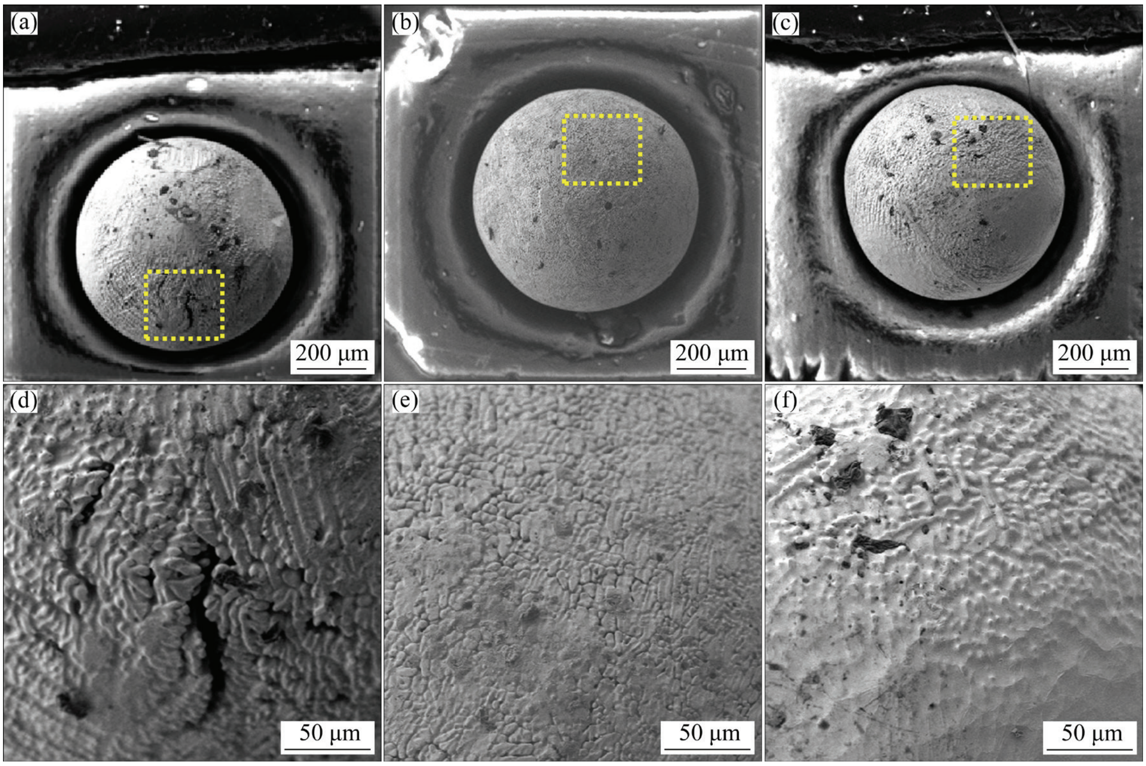

Fig. 3 Macroscopic morphology of solder joints with different Ag contents before rapid thermal shock: (a, d) SAC105; (b, e) SAC205; (c, f) SAC405

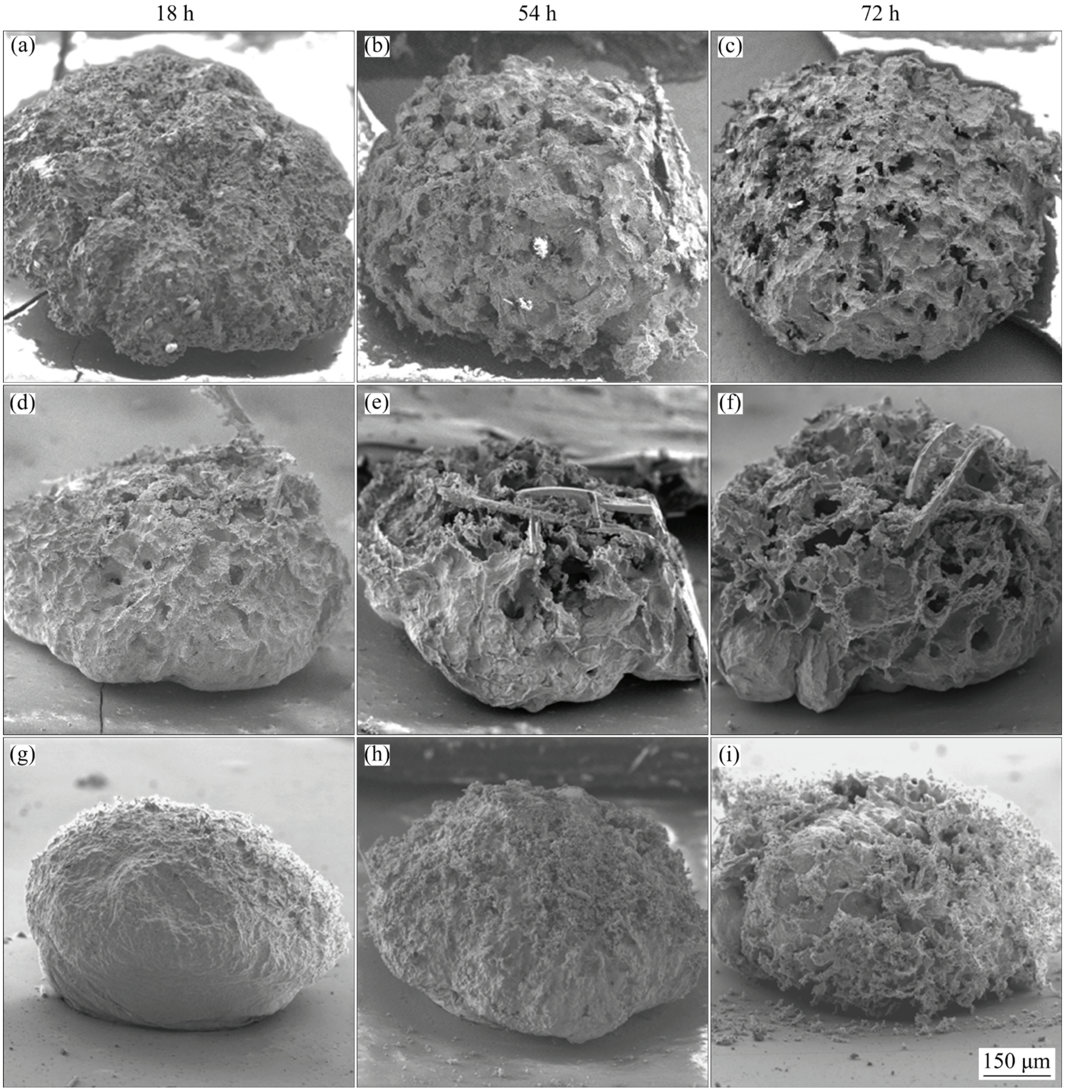

Fig. 4 Macroscopic morphology of solder joints with various silver contents after rapid thermal shock for various thermal shock durations: (a−c) SAC105; (d−f) SAC205; (g−i) SAC405

the growth in Ag_3Sn phase, which was thermodynamically more stable than the Sn matrix and reduced the solder ball oxidation rate [22]. This demonstrated that the increased Ag content of solder joints enhanced the oxidation resistance of solder joints, thus reducing the effect of rapid thermal shock on the macroscopic morphology of SAC solder joints.

In addition, the long strips of intermetallic compound (Cu_6Sn_5) found in the solder joints were brittle, which might affect the solder joints. Therefore, the exterior of the solder joint was etched to study the effect of internal IMC on solder joints with different Ag contents.

The internal IMC of solder joints with different Ag contents at different rapid thermal shock time is shown in Fig. 5. Large intermetallic compounds, Cu_6Sn_5 and Ag_3Sn, were observed inside all three solder joints. From the view point of elemental conservation, Cu in the solder was only 0.5%, which was insufficient to generate a large amount of Cu_6Sn_5, so Cu_6Sn_5 was caused by the reaction between Cu of the PCB and Sn of the solder. During reflow, many Cu atoms diffused from the PCB board to react with Sn atoms inside the solder. IMC grew upward along the temperature gradient created by bottom-up welding heating.

As the Ag content of the solder joint increased, the content of Cu_6Sn_5 decreased, while that of Ag_3Sn increased. The increased content of Ag inhibited the oxidation of solder joints. After reflowing, several thick and long hollow Cu_6Sn_5 appeared inside the

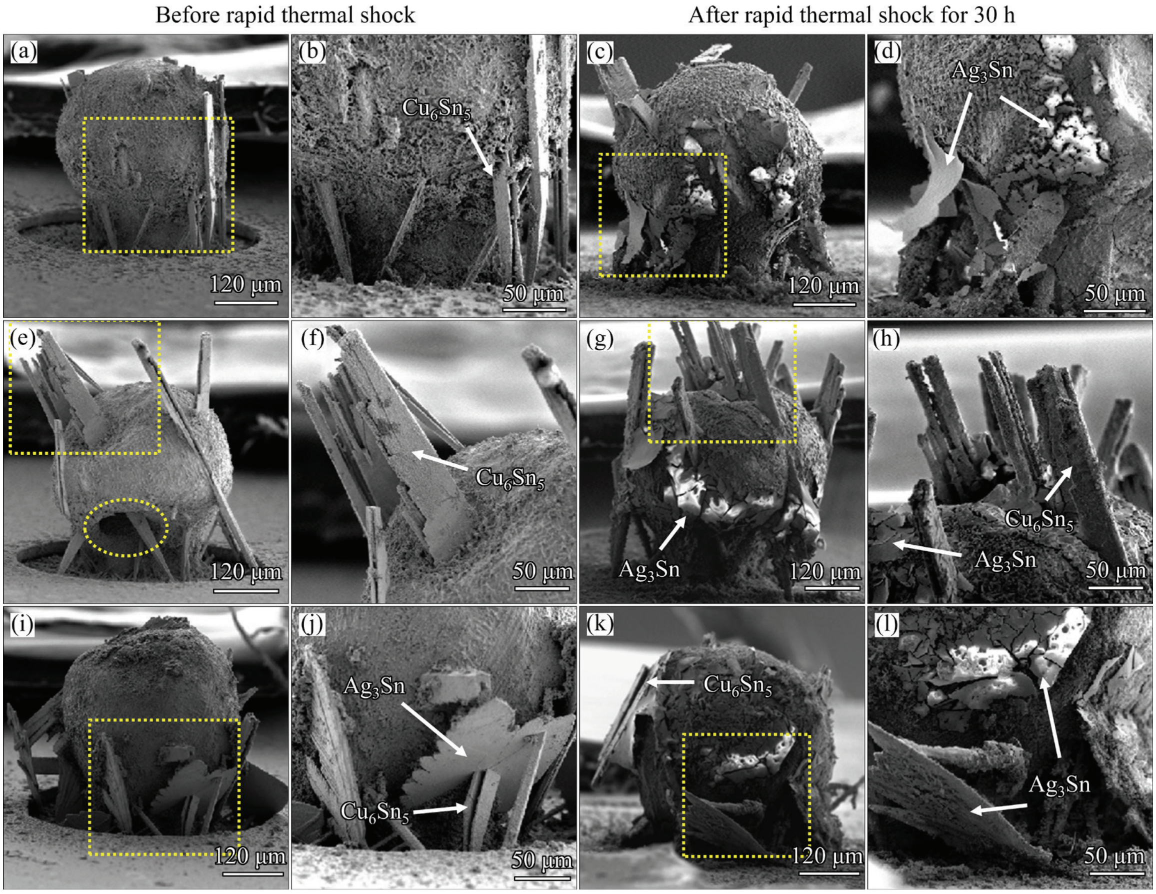

Fig. 5 Internal IMC morphology of solder joints before and after rapid thermal shock for 30 h: (a−d) SAC105; (e−h) SAC205; (i−l) SAC405

SAC105 solder joint and ran through the entire joint, reaching 36 μm at the widest point, as shown in Figs. 5(a, b). The rapid thermal shock was carried out for up to 36 h. The Cu_6Sn_5 size increased to 42 μm, and thin flakes of Ag_3Sn compounds appeared inside the solder joints, as shown in Figs. 5(c, d). Several long strips of Cu_6Sn_5 compound running through the entire solder joint also appeared inside SAC205, with the broadest part reaching 65 μm (Figs. 5(e, f)). A hole (shown as a yellow elliptical dashed line) was also observed, which might be a channel for the corrosion solution provided by the gap between the IMC and the solder joint during the corrosion process. This further indicated that the IMC inside the solder joint provided a channel for the oxidation of the solder joint during the rapid thermal shock process, which in turn affected the macroscopic shape of the joint. The Ag_3Sn that appeared inside the solder joint after 36 h aggregated into a larger size and more numerous thin flakes, as shown in Figs. 5(g, h). In the SAC105 and SAC205 solder joints, many tiny cracks appeared at the junction of Cu_6Sn_5 and solder, which were caused by the difference in thermal expansion coefficients between Cu_6Sn_5 [23] and solder and the extrusion stress generated by internal IMC growth [24]. Cracks allowed oxygen to seep into the solder joint, allowing the oxidation to extend to the inside of the joint, making it loose and porous.

Unlike SAC105 and SAC205 solder joints with low Ag content, a large amount of Ag_3Sn in the form of plates precipitated in the reflowed SAC405 solder joints, with approximately 2 μm in thickness, as shown in Figs. 5(i, j). The number of long strips of Cu_6Sn_5 and thin flakes of Ag_3Sn inside the SAC405 solder joint was significantly less than that in the SAC105 and SAC205 solder joints (Figs. 5(k, l)). This was due to the slight solubility of Ag in the solder; solder joints with a high Ag content were prone to bias Ag during reflow soldering, and the bias Ag and Sn in the solder together rapidly generated plate Ag_3Sn [21]. Ag_3Sn prevented the diffusion of Cu from the Cu substrate, thus inhibiting the formation of Cu_6Sn_5 [25]. Therefore, SAC405 solder joints had fewer cracks and holes and were less affected by oxidation. Most Ag was used to form large plates of Ag_3Sn, resulting in a decreased amount of Ag distributing inside the solder joint and, thus, a reduction of thin flakes of Ag_3Sn.

3.2 Evolution of interface IMC morphology

Figure 6 shows the microstructural change of IMC layers during rapid thermal shock for solder joints with different Ag contents. As the rapid thermal shock time increased, the IMC layer of the solder joint grew, and higher Ag contents corresponded to thicker IMC layers of the solder joint. SAC105 solder joints were distributed with jagged Cu_6Sn_5 after reflow, implying metallurgical bonding between the solder and the PCB board [26] (Fig. 6(a)). The interface was transformed from a monolayer Cu_6Sn_5 to a Cu_6Sn_5−Cu_3Sn bilayer structure after 18 h of rapid thermal shock, as shown in Fig. 6(b).

The interfacial IMC layer gradually thickened as the rapid thermal shock proceeded (Figs. 6(c, d)). After the reflow of SAC205 solder joints, the interfacial IMC layer had a jagged shape similar to that of SAC105, and the interfacial IMC layer also thickened with rapid thermal shock (Figs. 6(e−h)). The junction of the IMC with solder and Cu at the SAC405 solder joint interface after reflow was rough and contained Cu particles (Fig. 6(i)). This was due to the violent interfacial reaction during welding, where liquid Sn rapidly reacted with Cu to generate Cu_6Sn_5 compounds, resulting in some of Cu particles that failed to react with Sn in time being surrounded by Cu_6Sn_5 in the middle. It was demonstrated that the increased Ag content could reduce the interfacial energy and promote the reaction of Cu and Sn to form Cu_6Sn_5. Long strips of Ag_3Sn were found at the interface of IMC solder, and Cu_6Sn_5 was cross-grown with Ag_3Sn (Fig. 6(j)). After 54 h, Cu_6Sn_5 grew to 14.63 μm toward the interior of Ag_3Sn. The extension length of Cu_6Sn_5 was larger than that of other Cu_6Sn_5 layers with an average thickness of 8.74 μm in the same plane, as shown by the yellow dashed line in Fig. 6(k). The

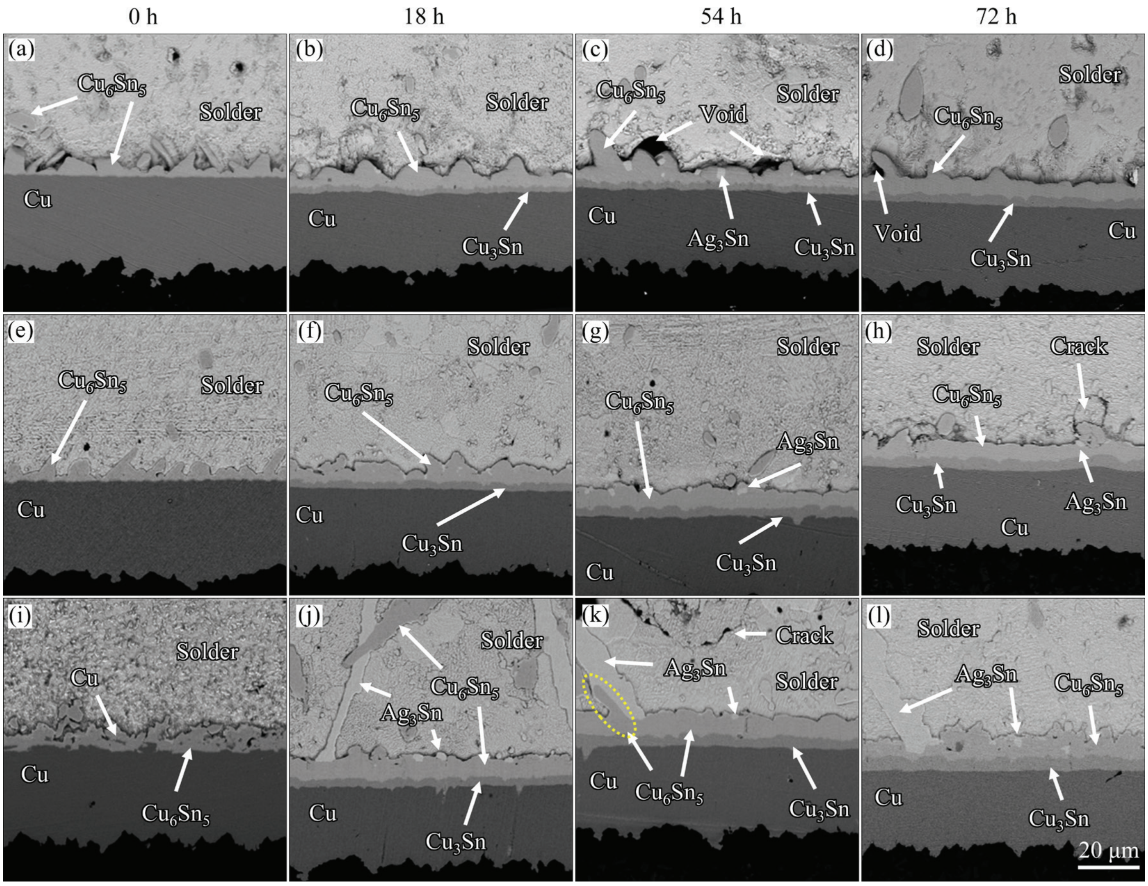

Fig. 6 Interfacial IMC morphology of solder joints after different rapid thermal shock durations: (a−d) SAC105; (e−h) SAC205; (i−l) SAC405

average thickness of the IMC layer of the SAC405 solder joint after 72 h was 12.02 μm, the average thicknesses of the IMC layer of the SAC105 and SAC205 solder joints with the same rapid thermal shock time were 7.97 and 8.2 μm, respectively, and the IMC layer of SAC405 was the thickest. This demonstrated that Ag under rapid thermal shock had a promotional effect on the growth of interfacial IMC layers.

Cracks appeared at the interface of the SAC205 and SAC405 solder joints, and coarse holes appeared at the interface of the SAC105 solder joints. This shows that the oxidation extended to the solder joint interface, and the SAC105 solder joint with the lowest Ag content was oxidized the most severely.

The exposed IMC grains of solder joints with different Ag contents at different rapid thermal shock time are shown in Fig. 7. With rapid thermal shock, the Cu_6Sn_5 grain size of the SAC105 solder joint increased, and the grain spacing decreased. The Cu_6Sn_5 grain boundaries were pinned with Ag_3Sn particles, as shown in Figs. 7(a−d). Compared to the Ag_3Sn particles in the SAC105 solder joints, SAC205 had a larger size and a higher number of Ag_3Sn particles (Figs. 7(f−h)). As shown in Fig. 7(i), the grain size of Cu_6Sn_5 with Ag_3Sn was larger in SAC405 solder joints after reflow than that in other Ag-containing solder joints. Because SAC405 is a peri-eutectic alloy, the excessive Ag content caused a large number of Ag atoms to precipitate during reflow soldering, forming a sizeable Ag_3Sn compound attached to the top of Cu_6Sn_5 (Figs. 7(j−i)), exacerbating Cu_6Sn_5 grain boundary distortion and thus generating larger Cu_6Sn_5 grains [27]. With rapid thermal shock, cracks appeared in the IMC grains of the solder joints with different Ag contents.

3.3 Growth mechanism of interfacial IMC layer

The variation in IMC layer thickness at the interface of solder joints with different Ag contents with rapid thermal shock time is shown in Fig. 8.

As shown in Fig. 8(a), the Cu_6Sn_5 layer at the interface of the solder joint grew in a parabolic manner, and the higher the Ag content of the solder joint, the thicker the Cu_6Sn_5 layer. The Cu_6Sn_5 layer thickness of the SAC405 solder joints was

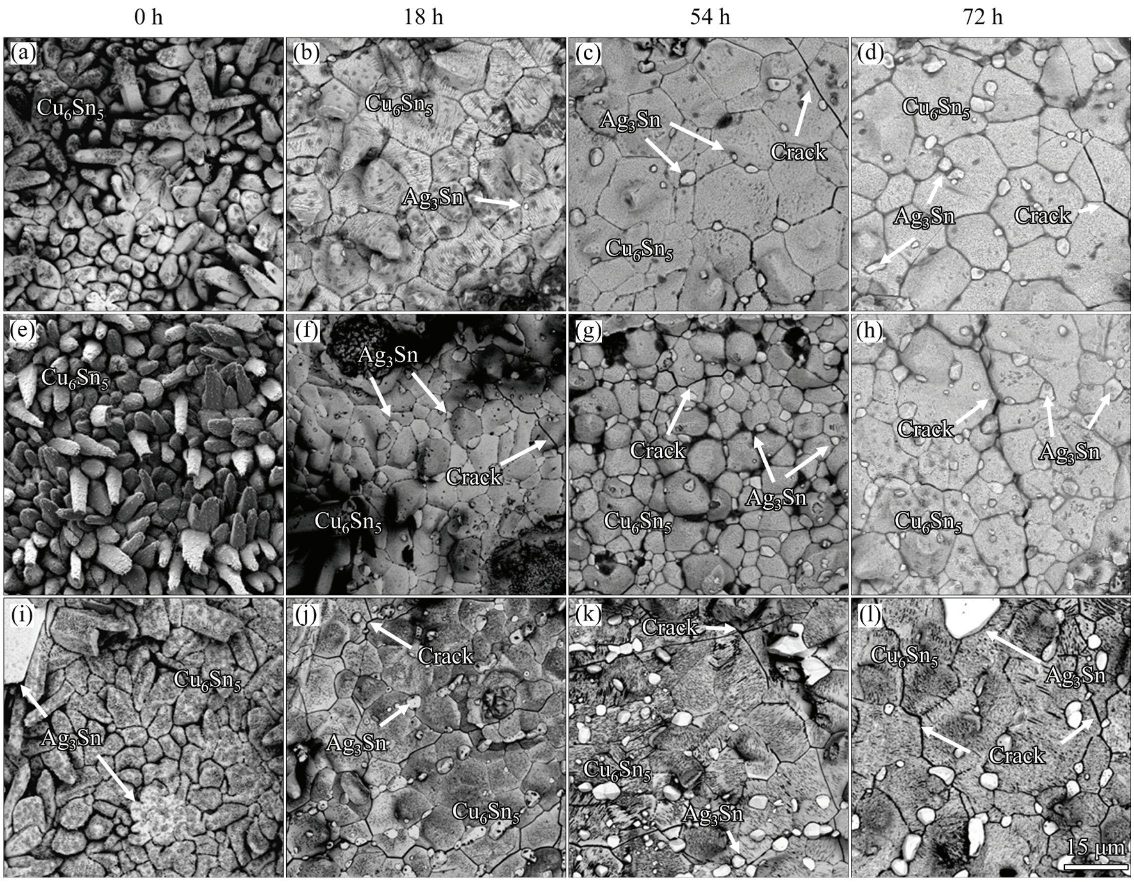

Fig. 7 Surface IMC morphology of solder joint after different rapid thermal shock durations: (a−d) SAC105; (e−h) SAC205; (i−l) SAC405

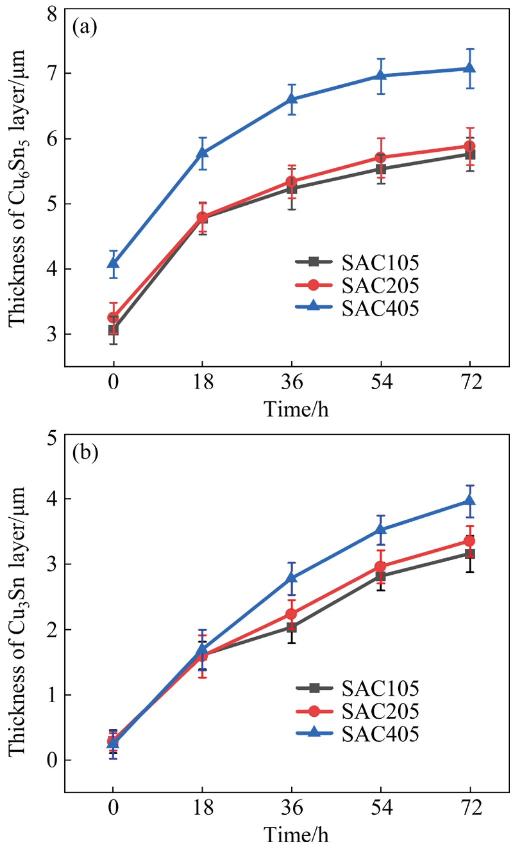

Fig. 8 Thickness evolution of different IMC layers under rapid thermal shock: (a) Cu_6Sn_5 layer; (b) Cu_3Sn layer

always larger than that of the other two. As shown in Fig. 8(b), the thickness of the Cu_3Sn layer was the same for all three solder joints within 18 h. However, after 18 h, the Cu_3Sn layer of the solder joints with higher Ag content grew faster.

To elucidate the growth mechanism of the interfacial IMC layer, an empirical power-law equation was used to describe the growth mechanism of the interfacial IMC layer [28]:

$$x=x_0+kt^n \tag{2}$$

$$k=\frac{x-x_0}{t^n} \tag{3}$$

$$n=\frac{\ln\left(x-x_0\right)}{\ln t} \tag{4}$$

where x_0 and x are the IMC layer thicknesses (μm) before and after thermal shock, respectively; k is the growth rate coefficient; t is the thermal shock time; n is the kinetic growth index.

The Sn-based solder interfacial IMC growth mechanism varies with n. At n=1, in the interfacial reaction control phase, the atomic diffusion rate controlled the IMC growth rate, and the growth rate was high. At n=1/2, the bulk diffusion-controlled phase, where the IMC growth rate was governed by the rate at which Cu atoms reached the IMC interface controlled the IMC growth rate, and the growth rate was low. At n=1/3, the grain boundary diffusion controlled the IMC growth rate, being related to the rate of Cu atoms crossing the grain boundary, and the growth rate was extremely low [29−31].

The growth kinetic index n and growth rate coefficient k were obtained by nonlinear regression analysis (Fig. 9 and Table 2).

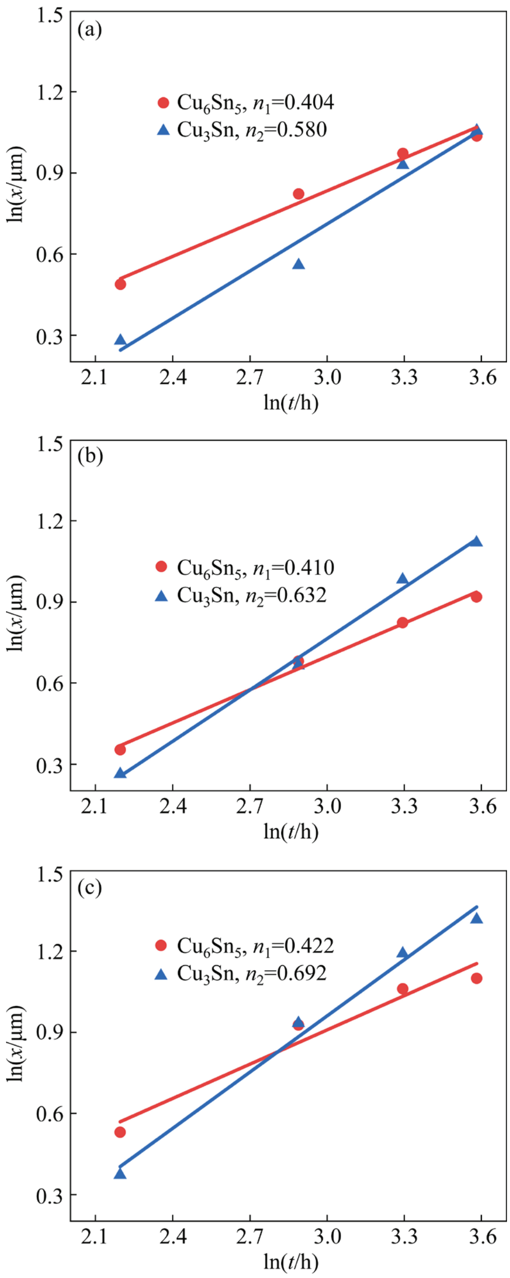

Fig. 9 Fitting results of IMC layer growth kinetic index for solder joints with different Ag contents: (a) SAC105; (b) SAC205; (c) SAC405

Table 2 Growth rate of IMC layer growth of solder joints

Solder	IMC layer	$k/(\mu m \cdot h^{-k})$	R^2
SAC105	Cu_6Sn_5	0.414±0.021	0.983
	Cu_3Sn	0.529±0.068	0.955
SAC205	Cu_6Sn_5	0.453±0.041	0.978
	Cu_3Sn	0.601±0.042	0.989
SAC405	Cu_6Sn_5	0.479±0.036	0.981
	Cu_3Sn	0.695±0.054	0.985

Figure 9 depicts the kinetic growth indices of Cu_6Sn_5 and Cu_3Sn layers for solder joints with different Ag contents. The n values of Cu_6Sn_5 for SAC105, SAC205, and SAC405 were 0.404, 0.410, and 0.422, respectively, indicating that both grain boundary diffusion and bulk diffusion controlled the growth of Cu_6Sn_5 layer in solder joints. As the Ag content increased, the effect of grain boundary diffusion control on Cu_6Sn_5 layer growth continued to drop, Cu_6Sn_5 layer growth was gradually controlled by body diffusion, and the growth rate of Cu_6Sn_5 layer in solder joints became higher because the increased Ag content reduced the interfacial energy at the grain boundary and promoted the diffusion of Cu atoms. The n values of Cu_3Sn for SAC105, SAC205 and SAC405 were 0.580, 0.632 and 0.692, respectively, and the growth of Cu_3Sn layer was controlled by both bulk diffusion and interfacial reaction. This indicated that the increased Ag content was more favorable to the growth of Cu_3Sn layer than Cu_6Sn_5 layer under rapid thermal shock.

Figure 9 indicates that the IMC layers at the interface are all dominated by bulk diffusion, so the IMC growth kinetic index of each layer is taken as 1/2 and linearly fitted with Eq. (3), and the results are given in Table 2. The growth rate coefficients of the Cu_6Sn_5 and Cu_3Sn layers increased with Ag content, confirming that Ag could promote IMC growth. In addition, the growth rate coefficients of Cu_3Sn under rapid thermal shock in different solder joints exceeded those of Cu_6Sn_5, indicating that Cu_3Sn grew faster than Cu_6Sn_5.

3.4 Shear strength and fracture behavior

Figure 10 shows the shear strength of solder joints with different Ag contents. The shear strength of SAC405 solder joints before rapid thermal shock was the highest, and that of SAC205 and SAC105 solder joints was the lowest. This was related to the diffusely distributed Ag_3Sn and dense Sn particles inside the solder joint, which could slow down slip generation during the shear process and thus improve the strength [32]. The shear strength of the solder joints all decreased linearly with rapid thermal shock duration. From 0 to 72 h, the shear strength of SAC405 solder joint decreased from 56.9 to 27.6 MPa, by 52.24%, the shear strength of SAC205 solder joint dropped from 51.7 to 33.1 MPa, by 36.03%, and the shear strength of SAC105 solder joint decreased from 49.5 to 29.8 MPa, by 39.81%.

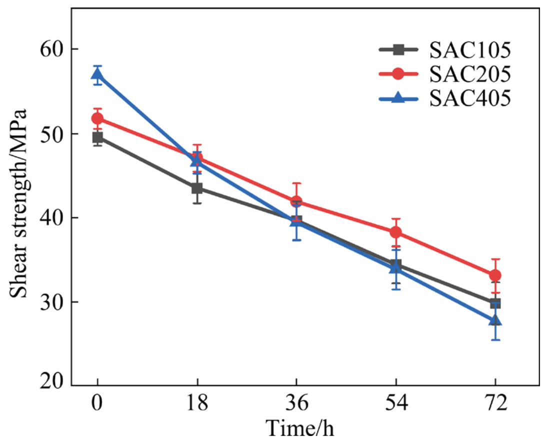

Fig. 10 Shear strength of solder joints with different Ag contents for various rapid thermal shock durations

Figure 11 shows the fracture profile of three types of solder joints after reflowing. The SAC105 solder joint fracture surface was relatively flat, and there were a large number of dense small dimples inside, as shown in Figs. 11(a, d). The SAC205 solder joints had many unevenly sized dimples (Figs. 11(b, e)). When the Ag content increased to 4 wt.%, the fracture surface of the solder joint was uneven and had coarse holes and dimples, as shown in Figs. 11(c, f). Ag_3Sn probably left coarse holes, with coarse tough nests indicating high toughness of SAC405, consistent with the highest shear strength of this solder joint. The fracture morphology of these three types of solder joints indicates that the reflowed solder joints were fractured inside the solder joints, and their fracture mode was ductile.

The fracture morphology of solder joint with different Ag contents with different rapid thermal shock durations is shown in Fig. 12. With rapid

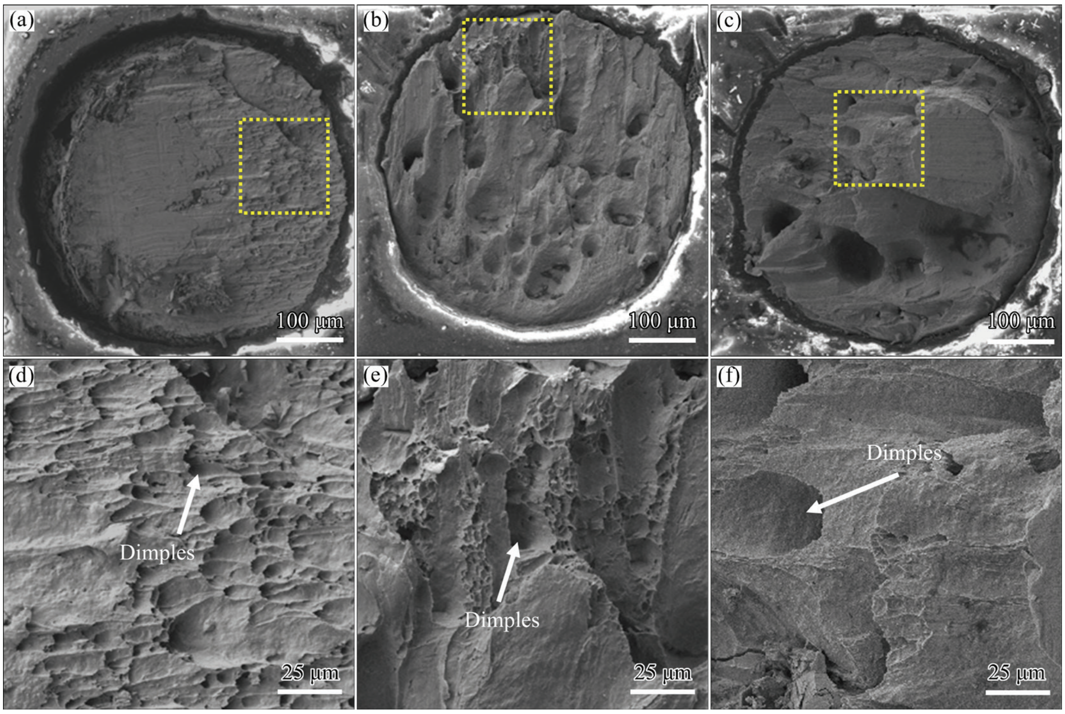

Fig. 11 Fracture profile of solder joints with different Ag contents before rapid thermal shock: (a, d) SAC105; (b, e) SAC205; (c, f) SAC405

thermal shock, the fracture mode of the solder joints converted from ductile fracture to brittle fracture, and the transition time of the fracture mode of the solder joints first increased and then dropped.

The rapid thermal shock caused the area of the SAC105 solder joint fracture in the IMC layer to increase, and at 72 h, the entire lower half of the SAC105 solder joint was cracked, indicating low reliability of the solder joint at this time (Figs. 12(a−c)). At 18 h, the SAC205 solder joint fractured inside the joint, and the fracture had many tear ribs and dimples, which had more obvious toughness characteristics than the SAC105 joint (Figs. 12(d−f)). The SAC405 solder joint fracture mode transition time was shorter than that of the other two solder joints. The solder joint even broke between Cu_6Sn_5 and Cu_3Sn in the IMC layer after 72 h (Figs. 12(h, i)). TIAN et al [33] have studied the reliability of BGA solder joints with Sn−3.0Ag−0.5Cu solder in conventional thermal shock tests. Their results showed that the fracture mode of the SAC305 solder joint transformed from ductile fracture to brittle after 312.5 h of thermal shock, and the Cu_3Sn phase appeared in the fracture after 375 h. In this study, the fracture mode of different solder joints completed the transition from ductile fracture to brittle fracture within 72 h. The fracture of SAC405 solder joints under rapid thermal shock was similar to that of SAC305 joints under conventional thermal shock but with a higher transition rate. This indicated that the final damage effect of rapid thermal shock on solder joints was similar to that of conventional thermal shock, but the damage occurred much faster.

Different fracture mode transition time of solder joints with different Ag contents was related to the thickness of the IMC layer of solder joint and the oxidation behavior during rapid thermal shock. For SAC105 solder joints, the lowest Ag content aggravated the oxidation of SAC105 joints. This caused the solder to become loose and porous, significantly reducing the solder−interface bonding. The high Ag content of SAC405 solder joints facilitated the growth of IMC layers, making it easy for the joints to fracture on the brittle IMC layers during shear. Additionally, because Cu_3Sn was much brittler than Cu_6Sn_5 [34] and was more likely to fracture due to the difference in thermal expansion coefficients between the two, the fracture mode transition time of SAC405 joints was less than that of SAC105 joints. The shear strength of SAC405 joints after 72 h was lower than that of SAC105 joints. The Ag content of the SAC205 solder joints was between that of SAC105 and SAC405 joints,

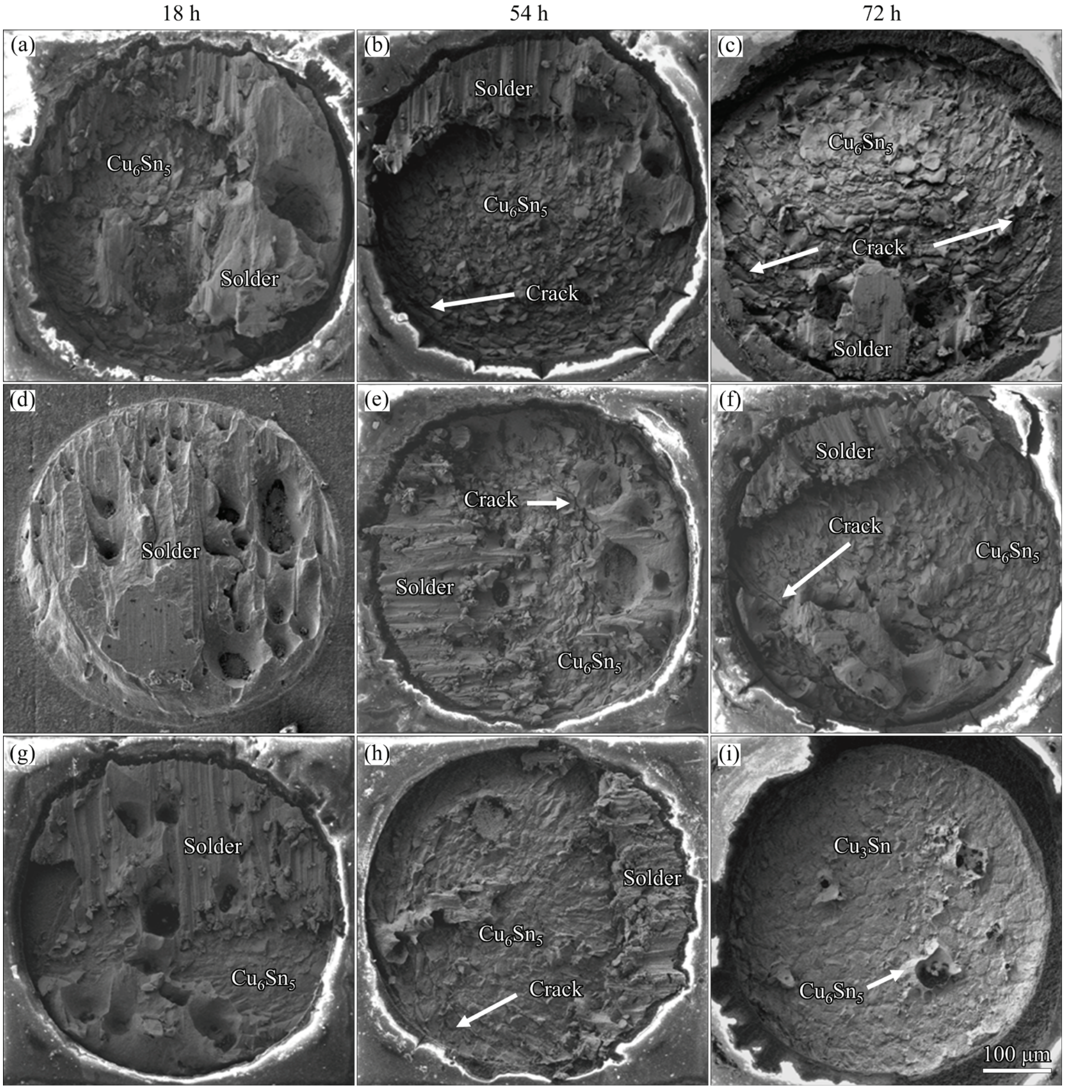

Fig. 12 Fracture profile of solder joint with different Ag contents with different rapid thermal shock durations: (a−c) SAC105; (d−f) SAC205; (g−i) SAC405

inhibiting the solder oxidation compared to that of SAC105 joints and making the IMC layer thinner than that of SAC405. Therefore, SAC205 had the longest fracture mode transition time and the highest shear strength after rapid thermal shock.

4 Conclusions

(1) The increased Ag content of the solder joint reduced the size of the Sn particles in the solder joint, hindering the diffusion of oxidation and promoting the Ag_3Sn phase generation, thus improving the corrosion resistance of the solder joint.

(2) As the Ag content of the solder joint increased, plate-like Ag_3Sn appeared inside the solder joint after rapid thermal shock, and long strips of Cu_6Sn_5 were reduced. Long strips of Cu_6Sn_5 contributed to the generation of holes and cracks in the solder joint, aggravating the oxidation of solder joint. The Ag_3Sn plate hindered the diffusion of Cu atoms, thus reducing the generation of long strips of Cu_6Sn_5.

(3) The increased Ag content promoted the growth of interfacial IMCs under rapid thermal shock. The growth of the Cu_6Sn_5 layer in solder joints upon rapid thermal shock was controlled by grain boundary and bulk diffusion. In contrast, the growth of the Cu_3Sn layer was controlled by both bulk diffusion and interfacial reaction.

(4) The increased Ag content before rapid thermal shock improved the shear strength of the solder joint. However, the increased Ag content after rapid thermal shock promoted the fracture

mode transition from ductile to brittle fracture in the solder joints, resulting in the most significant decrease in the shear strength of SAC405 joints.

CRediT authorship contribution statement

Chen PENG: Investigation, Methodology, Writing − Original draft, Visualization; **Shan-lin WANG:** Resources, Writing − Review & editing, Funding acquisition; **Ming WU:** Data acquisition, Writing − Review & editing, Experiments; **Li-meng YIN:** Resources, Supervision; **Yu-hua CHEN:** Resources, Funding acquisition; **Ke-jiang YE:** Software, Experiments; **Wei-zheng CHEN:** Visualization, Experiments; **Ti-ming ZHANG:** Resources, Methodology; **Ji-lin XIE:** Resources, Supervision.

Declaration of competing interest

The authors declare that they have no known competing financial interests or personal relationships that could have appeared to influence the work reported in this paper.

Acknowledgments

The authors are grateful for the financial support from the National Natural Science Foundation of China (No. 51965044).

References

[1] EL-DALY A A, FAWZY A, MOHAMAD A Z, EL-TAHER A M. Microstructural evolution and tensile properties of Sn−5Sb solder alloy containing small amount of Ag and Cu [J]. Journal of Alloys and Compounds, 2011, 509(13): 4574−4582.

[2] AAMIR M, MUHAMMAD R, TOLOUEI-RAD M, GIASIN K, SILBERSCHMIDT V V. A review: Microstructure and properties of tin-silver-copper lead-free solder series for the applications of electronics [J]. Soldering & Surface Mount Technology, 2019, 32(2): 115−126.

[3] BAATED A, KIM K S, SUGANUMA K, HUANG S, JURCIK B, NOZAWA S, UESHIMA M. Effects of reflow atmosphere and flux on Sn whisker growth of Sn−Ag−Cu solders [J]. Journal of Materials Science: Materials in Electronics, 2010, 21(10): 1066−1075.

[4] QIN Yi, WILCOX G D, LIU Chang-qing. Electrodeposition and characterisation of Sn−Ag−Cu solder alloys for flip-chip interconnection [J]. Electrochimica Acta, 2010, 56(1): 183−192.

[5] TEJA M B K, SHARMA A, DAS S, DAS K. A review on nanodispersed lead-free solders in electronics: Synthesis, microstructure and intermetallic growth characteristics [J]. Journal of Materials Science, 2022, 57(19): 8597−8633.

[6] ZHAI Xin-meng, LI Yue-feng, ZOU Jun, SHI Ming-ming, YANG Bo-bo, LI Yang, GUO Chun-feng, HU Rong-rong. Effect of soldering temperature on the reliability of Sn−Ag−Cu lead-free solder joints [J]. Journal of Electronic Materials, 2021, 50(3): 869−880.

[7] LUO Ting-bi, CHEN Zhuo, HU An-min, LI Ming. Study on melt properties, microstructure, tensile properties of low Ag content Sn−Ag−Zn Lead-free solders [J]. Materials Science and Engineering A, 2012, 556: 885−890.

[8] SHARMA A, XU D E, CHOW J, MAYER M, SOHN H R, JUNG, J P. Electromigration of composite Sn−Ag−Cu solder bumps [J]. Electronic Materials Letters, 2015, 11(6): 1072−1077.

[9] KARIYA Y, HOSOI T, TERASHIMA S, TANAKA M, OTSUKA M. Effect of silver content on the shear fatigue properties of Sn−Ag−Cu flip-chip interconnects [J]. Journal of Electronic Materials. 2004, 33(4): 321−328.

[10] SYED A, SCANLAN J, CHA S W, KANG W J, SOHN E S, KIM T S, RYU C G. Impact of package design and materials on reliability for temperature cycling, bend, and drop loading conditions [C]//2008 58th Electronic Components and Technology Conference. Lake Buena Vista, FL, USA: IEEE, 2008: 1453−1461.

[11] CHE Fa-xing, POH E C, ZHU W H, XIONG B S. Ag content effect on mechanical properties of Sn−*x*Ag−0.5Cu solders [C]//2007 9th Electronics Packaging Technology Conference. Singapore: IEEE, 2007: 713−718.

[12] LI Xue-mei, SUN Feng-lian, ZHANG Hao, LIU Meng, FAN Rui. Interfacial reactions in molten state micro solder joints under current stressing [J]. Journal of Alloys and Compounds, 2018, 739: 388−392.

[13] LIU Cong, XIA Da-quan, TIAN Mi-zhe, CHEN Shi-qi, GAN Gui-sheng, DU Yun-fei, LIU Xin, JIANG Zhao-qi, WU Yi-ping, MA Yan-long. Fatigue cracking growth of SAC305 solder ball under rapid thermal shock [J]. Engineering Fracture Mechanics, 2022, 259: 108414.

[14] PERPIÑÀ X, PITON M, MERMET-GUYENNET M, JORDÀ X, MILLÁN J. Local thermal cycles determination in thermosyphon-cooled traction IGBT modules reproducing mission profiles [J]. Microelectronics Reliability, 2007, 47(9): 1701−1706.

[15] JIANG Nan, ZHANG Liang, LIU Zhi-quan, SUN Lei, LONG Wei-min, HE Peng, XIONG Ming-yue, ZHAO Meng. Reliability issues of lead-free solder joints in electronic devices [J]. Science and Technology of Advanced Materials, 2019, 20(1): 876−901.

[16] LALL P, BHAT C, HANDE M, MORE V, VAIDYA R, GOEBEL K. Prognostication of residual life and latent damage assessment in lead-free electronics under thermomechanical loads [J]. IEEE Transactions on Industrial Electronics, 2011, 58(7): 2605−2616.

[17] ZHANG Peng-fei, WANG De-cheng, CHENG Peng, SHAO Chen-xi, ZHU Wei, ZHOU Jun-ying, HUANG Ji-hua. Microstructure, mechanical properties and corrosion behavior of 65Mn tape-steel via electromagnetic induction heating [J]. Materials Today Communications, 2022, 30: 103175.

[18] KIM J, JO Y, LEE K. Comparison with reliability of low Ag solder ball by thermal shock and cycling tests [C]//2016 6th Electronic System-Integration Technology Conference (ESTC). Grenoble, France: IEEE, 2016: 1−4.

[19] TIAN Mi-zhe, GAN Gui-sheng, CAO Hua-dong, YANG Dong-hua, JIANG Liu-jie, XIA Da-quan, SUN Peng-fei, LIU Xin, WU Yi-ping. Effect of rapid thermal fatigue on

microstructure and properties of Sn3.0Ag0.5Cu/Cu solder bumps [C]//2020 21st International Conference on Electronic Packaging Technology (ICEPT). Guangzhou: IEEE, 2020: 1−4.

[20] CHEN Ji-bing, YIN Yan-fang, YE Jian-ping, WU Yi-ping. Investigation on fatigue behavior of single SnAgCu/SnPb solder joint by rapid thermal cycling [J]. Soldering & Surface Mount Technology, 2015, 27(2): 76−83.

[21] TUNTHAWIROON P, KANLAYASIRI K. Effects of Ag contents in Sn−*x*Ag lead-free solders on microstructure, corrosion behavior and interfacial reaction with Cu substrate [J]. Transactions of Nonferrous Metals Society of China, 2019, 29(8): 1696−1704.

[22] OSORIO W R, PEIXOTO L C, GARCIA L R, GARCIA A, SPINELLI J E. The effects of microstructure and Ag3Sn and Cu6Sn5 intermetallics on the electrochemical behavior of Sn−Ag and Sn−Cu solder alloys [J]. International Journal of Electrochemical Science, 2012,7(7): 6436−6452.

[23] ZHONG Ying, AN Rong, WANG Chun-qing, ZHENG Zhen, LIU Zhi-Quan, LIU Chin-hung, LI Cai-fu, KIM T K Y, JIN Sung-ho. Low temperature sintering Cu6Sn5 nanoparticles for superplastic and super-uniform high temperature circuit interconnections [J]. Small, 2015, 11(33): 4097−4103.

[24] WU Ming, WANG Shan-lin, YIN Li-meng, CHEN Yu-hua, HONG Min, SUN Wen-jun, YAO Zong-xiang, NI Jia-ming, LU Peng, ZHANG Ti-ming, XIE Ji-lin. Oxidation behavior and intermetallic compound growth dynamics of SAC305/Cu solder joints under rapid thermal shock [J]. Transactions of Nonferrous Metals Society of China, 2023: 3054−3066.

[25] YU D Q, WANG L, WU C M L., LAW C M T. The formation of nano-Ag3Sn particles on the intermetallic compounds during wetting reaction [J]. Journal of Alloys and Compounds, 2005, 389(1): 153−158.

[26] DEPIVER J A, MALLIK S, AMALU E H. Effective solder for improved thermo-mechanical reliability of solder joints in a ball grid array (BGA) soldered on printed circuit board (PCB) [J]. Journal of Electronic Materials, 2021, 50(1): 263−282.

[27] LIASHENKO O Y, LAY S, HODAJ F. On the initial stages of phase formation at the solid Cu/liquid Sn-based solder interface [J]. Acta Materialia, 2016, 117: 216−227.

[28] XIONG Ming-yue, ZHANG Liang. Interface reaction and intermetallic compound growth behavior of Sn−Ag−Cu lead-free solder joints on different substrates in electronic packaging [J]. Journal of Materials Science, 2019, 54(2): 1741−1768.

[29] BAO Ni-fa, HU Xiao-wu, LI Qing-lin, LI Shuang. Effect of Cu concentration on the interfacial reactions between Sn−*x*Cu solders and Cu substrate [J]. Materials Research Express, 2019, 6(7): 076310.

[30] HUANG M L, YANG F. Size effect model on kinetics of interfacial reaction between Sn−*x*Ag−*y*Cu solders and Cu substrate [J]. Scientific Reports, 2014, 4(1): 7117.

[31] KIM D G, JUNG S B. Interfacial reactions and growth kinetics for intermetallic compound layer between In−48Sn solder and bare Cu substrate [J]. Journal of Alloys and Compounds, 2005, 386(1): 151−156.

[32] TERASHIMA S, TANAKA M, TATSUMI K. Thermal fatigue properties and grain boundary character distribution in Sn−*x*Ag−0.5Cu (*x*=1, 1.2 and 3) lead free solder interconnects [J]. Science and Technology of Welding and Joining, 2008, 13(1): 60−65.

[33] TIAN Ru-yu, HANG Chun-jin, TIAN Yan-hong, ZHAO Li-you. Growth behavior of intermetallic compounds and early formation of cracks in Sn−3Ag−0.5Cu solder joints under extreme temperature thermal shock [J]. Materials Science and Engineering A, 2018, 709: 125−133.

[34] DING Chao, WANG Jian, LIU Tian-han., QIN Hong-bo, YANG Dao-guo, ZHANG Guo-qi. The mechanical properties and elastic anisotropy of η'-Cu_6Sn_5 and Cu3Sn intermetallic compounds [J]. CRYSTALS, 2021, 11(12): 1562.

银含量对快速热冲击下 Sn−*x*Ag−0.5Cu 焊点显微组织和力学性能的影响

彭 晨[1]，王善林[1]，吴 鸣[1,2]，尹立孟[3]，陈玉华[1]，叶科江[1]，陈维政[1]，张体明[1]，谢吉林[1]

1. 南昌航空大学 江西省航空构件成形与连接重点实验室，南昌 330036；

2. 江西省智能产业技术创新研究院，南昌 330200；

3. 重庆科技学院 冶金与材料工程学院，重庆 401331

摘 要：使用高频感应加热设备研究 Ag 含量对快速热冲击下 Sn−*x*Ag−0.5Cu 焊点的显微组织和剪切强度的影响。结果表明，Ag 含量的增加使焊点表面更致密光滑，减少焊点内部长条状 Cu_6Sn_5 金属间化合物(IMC)的产生，从而提高焊点的抗氧化性。Ag 能够加快焊点界面 IMC 层的生长速度，Cu_6Sn_5 层的生长速度由体扩散和晶界扩散共同决定，Cu_3Sn 层的生长速度由体扩散和界面反应共同决定。在快速热冲击环境下，焊点的断裂模式从韧性断裂转变为脆性断裂，而高 Ag 含量使得焊点的断裂模式转变时间更短，降低焊点的抗热疲劳性能。

关键词：Ag 含量；快速热冲击；Sn−Ag−Cu；焊点；生长动力学；断裂模式

(Edited by Xiang-qun LI)